Organic–Inorganic Hybrid Materials. II. Chain Mobility and Stability of Polysiloxaneimide–Silica Hybrids

K. H. WU,[1] T. C. CHANG,[2*] J. C. YANG,[3] H. B. CHEN[3]

[1] Chemical Service of the Republic of China Army, P.O. Box 90615, Lung-Tang, Taiwan, Republic of China

[2] Department of Applied Chemistry, Chung Cheng Institute of Technology, Tahsi, Taoyuan, Taiwan 33509, Republic of China

[3] Chemical Systems Research Division, Chung Shan Institute of Science and Technology, Taoyuan, Taiwan 32526, Republic of China

Received 12 January 1999; accepted 2 February 2000

ABSTRACT: Polysiloxaneimide–silica hybrid materials (PSI-SiO_2) were obtained using the sol–gel technique by polycondensation of tetramethoxysilane (TMOS) in a polyamic acid solution. IR, ^{29}Si- and ^{13}C-NMR spectroscopy, and thermogravimetric analysis were used to study hybrids containing various proportions of TMOS and hydrolysis ratios. The morphology, dynamics, and thermal stability of the hybrids were investigated. The chain mobility of the hybrids was investigated by spin–spin relaxation time (T_2) measurements. The apparent activation energy (E_a) for degradation of the hybrids in air was studied by the van Krevelen method. The T_2 value was independent of the silica content whereas that of the E_a decreased as silica content increased. © 2000 John Wiley & Sons, Inc. J Appl Polym Sci 79: 965–973, 2001

Key words: polysiloxaneimide; silica; hybrids; spin–spin relaxation; degradation; activation energy of degradation

INTRODUCTION

Organic–inorganic hybrids are attractive materials with heat resistance, mechanical and electrical properties, and radiation resistance.[1] Organic polymers combined with inorganic oxides using variations of the sol–gel method have become prevalent during the past decade as a means of preparing organic–inorganic hybrid materials.[2] Many polymers, such as poly(dimethylsiloxane),[3] poly(tetramethylene oxide),[4] poly(oxyethylene),[5] poly(ether ketone),[6] poly(methyl methacrylate),[7] and polyimide,[8–19] have been used in this kind of synthesis.

Polyimides are of great interest for high-performance applications because they exhibit outstanding dielectric and mechanical properties at elevated temperatures.[20] However, polyimides exhibit relatively high values of water sorption and coefficients of thermal expansion, impeding electronic applications.[21] A silica (SiO_2) exhibiting very low values of water sorption and coefficient of thermal expansion would be more suited for electronic applications. But the dielectric properties, planarizability, and patternability of silica are inferior to polyimides. Polyimide–silica hybrid materials offer favorable properties of both the polyimides and silica and are therefore in great demand.

Two main procedures have been used to prepare polyimide–silica hybrids. The first uses a

Correspondence to: T. C. Chang.

Contract grant sponsor: National Science Council of the Republic of China; contract grant number: NSC 88-2113-M014-004.

Journal of Applied Polymer Science, Vol. 79, 965–973 (2001)

mixture of a tetrafunctional silicon alkoxide and the polyimide precursors to produce composite materials.[8–14] The second creates bonding sites between the polymer backbone and the silica.[15–19] A nanoscale polyimide–silica hybrid for fine-line metallization has been reported.[8] Nandi et al.[9] produced polyimide–silica hybrids by mixing solutions of pyromellitic anhydride, diaminodiphenyl ether, and silicon tetraalkoxides. They rely only on physical interactions between the inorganic and organic phases and accordingly become opaque at low weight percentages of silica because of phase separation on the micron scale. Breval et al.[10] found that a silica content near 9 vol % yields a well-mixed polyimide–silica hybrid that is homogeneous down to nanometer scale and has good planarization characteristics. On the other hand, Morikawa et al.[11] prepared the polyimide–silica hybrid materials by the polyamic acid triethylamine salt (PAA-NEt_3) in *N*,*N*-dimethylacetamide (DMAc) and obtained a macrophase separation. They subsequently prepared the polyimide–silica hybrid films by PAA-NEt_3 in methanol. In the latter case the size of the silica globules was controlled by the drying temperature of the cast films.[12] Gaw et al.[13] further prepared the polyimide–silica hybrids by a modified high pressure sol–gel reaction of a metal alkoxide and a monomer salt. The authors found that the incorporation of siloxane amine into the polyimide backbone homogenized the composites and the silica content did not affect the polymer decomposition temperature. Goizet et al.[14] obtained polyimide–silica composite films using the sol–gel process by condensation of metal alkoxide in a PAA solution. They showed the influence of the silica and water content on the condensation kinetics.

Investigations of polyimide–silica hybrids were recently carried out on their microstructure,[14] morphology,[17] optical properties,[18] and thermal stability.[19] However, there are very few articles on the apparent activation energy (E_a) of thermooxidative degradation and the dynamics of polyimide–silica hybrids. In the present study polysiloxaneimide–silica hybrids (PSI-SiO_2) were prepared by the sol–gel technique, and the effect of the alkoxysilane solution composition on the structure and thermooxidative stability of the hybrids was investigated. To understand the dynamics of the hybrids, we measured spin–spin relaxation times (T_2) of the siloxane and imide segments in hybrids. Furthermore, the thermooxidative stability of hybrids was measured by mean of thermogravimetric analysis (TGA). The

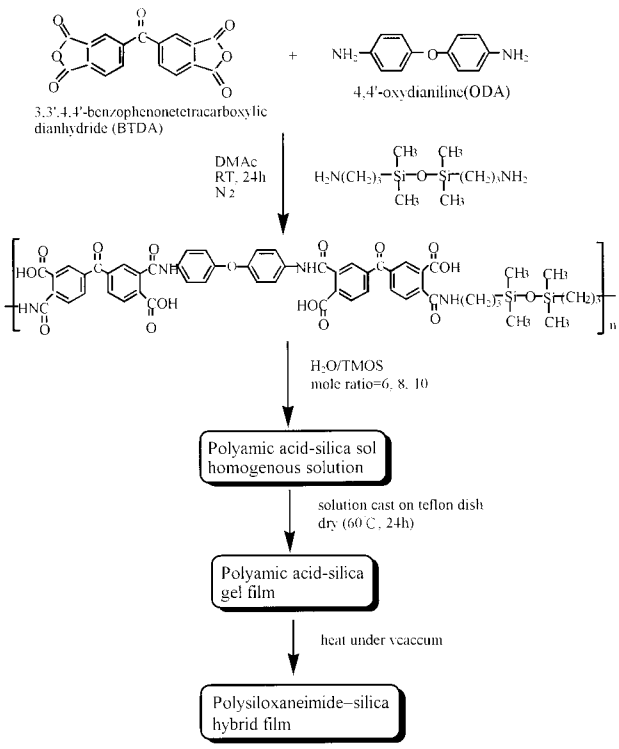

Scheme 1 The general synthetic scheme of the PSI-SiO_2 hybrid materials.

E_a values were evaluated by the van Krevelen method.[22]

EXPERIMENTAL

Materials

3,3′,4,4′-Benzophenone tetracarboxylic dianhydride (BTDA) and oxydianiline (ODA) were obtained in high purity from Tokyo Chemical Industry Co. and dried under a vaccum for 24 h at 120 and 70°C, respectively. Tetramethoxysilane (TMOS) and diaminopropyl tetramethyl-disiloxane (DAPrTMDS) were obtained from Gelset, Inc., and used without further purification. DMAc (Aldrich) was distilled under a vacuum. Deionized water (18 MΩ) was used for their hydrolysis.

Preparation of PSI-SiO_2 Hybrids

The general synthetic scheme of the PSI-SiO_2 hybrid materials is depicted in Scheme 1. The preparation of PAA with a concentration of 15% solids by weight in the solvent was conducted at room temperature under nitrogen. A solution of ODA in DMAc was added to a solution of BTDA in

Table I Experimental Conditions for Polysiloxaneimide–Silica Hybrid Materials

Hybrids	TMOS (wt %)	H_2O/TMOS (mol ratio)	SiO_2[a] (wt %)
A: 6B	0	0	7
B: 6B-30	30	6	26
C: 6B-50	50	6	38
D: 6B-70	70	6	50
E: 8B-50	50	8	36
F: 10B-50	50	10	36

BTDA (0.024 mol), ODA (0.012 mol), and DAPrTMDS (0.012 mol) were used.

[a] The silica content indicates the final weight percent of residue obtained after heating at 800°C in air.

DMAc in a round-bottomed flask with a stirring magnet. After 30 min the DAPrTMDS was added and the clear solution was stirred for 24 h. The resulting viscous, pale orange PAA solution was then obtained.

The desired amounts of water and TMOS were added to the PAA solution and stirred for an additional 24 h at room temperature. The resulting homogeneous solution was poured onto a Teflon dish. After drying at 60°C for 24 h under atmospheric pressure, the film was then heated 3 h at 100°C, 3 h at 200°C, 2 h at 250°C, and 2 h at 300°C under a vacuum. Three different hydrolysis ratios (molar ratio of $[H_2O]/[TMOS] = 6$, 8, and 10) were used. Hybrid materials were designated so that, for example, 6B-30, 6B-50, and 6B-70 denote PAA added with about 30, 50, and 70 wt % TMOS, respectively, in which the molar ratio of $[H_2O]/[TMOS]$ was 6. The PSI hybrid 6B without the addition of TMOS and water was synthesized via a similar procedure for comparison. The experimental conditions for hybrid materials discussed in this article are shown in Table I.

Characterization of PSI-SiO_2 Hybrids

The IR spectra of samples dispersed in dry KBr pellets were recorded between 4000 and 400 cm^{-1} on a Bomen DA 3.002 FTIR spectrometer. Imidization was confirmed by the IR spectra of the samples. In addition, the frequency shift of the carbonyl stretching band was used to analyze the hydrogen bonding between the O—H group of the silica and the C═O group of the polyimide. The ^{29}Si-NMR and ^{13}C-NMR spectra of the solid hybrids were determined (Bruker MSL-400) by using the cross-polarization combined with magic angle spinning (CP/MAS) technique. The ^{29}Si-NMR provides a unique way to follow the hydrolysis and condensation reactions of silicon alkoxides. The nomenclatures of Q^i is taken from Glaser and Wilkes.[4] The Q^i denotes species that have no organic side group and i refers to the number of —O—Si groups bound to the silicon atom of interest. The proton spin–spin relaxation time (T_2) was measured at room temperature via solid-state ^{13}C-NMR using the pulse sequence described by in the literature.[23,24] The characteristics and kinetics of degradation of the hybrids were measured by a Perkin–Elmer TGA-2 at a heating rate of 10°C/min under air and nitrogen. The sample weight was about 10 mg, and the gas flow rate was kept at 100 mL/min.

RESULTS AND DISCUSSION

Materials Characterization

The hybrids presented the silanol group formed during the hydrolysis of the alkoxy groups (Si—OCH_3) from TMOS and that induced crosslinked 3-dimensional (3-D, Q^i) network materials. Evidence for the formation of hybrid network materials was provided by FTIR and solid-state ^{29}Si- and ^{13}C-NMR. The theoretical schematic structures of the hybrids are shown in Figure 1.

The IR spectra of hybrid materials containing various proportions of silica are shown in Figure 2. All hybrids present the characteristic imide peaks at 1776 (imide C═O symmetric stretching), 1717 (imide C═O asymmetric stretching), 1382 (C—N stretching), and 720 cm^{-1} (imide ring deformation). The Si—O—Si vibration (1077 cm^{-1}) is small in the 6B hybrid [Fig. 2(A)], but this absorption band is broader with increasing silica content for other hybrids [Fig. 2(B–F)]. This implies the condensation of the already hydrolyzed TMOS to form the 3-D Si—O—Si network.[25,26] The absorptions in the 3700–3200 cm^{-1} range are the characteristic band of silanol groups (Si—OH) that are formed during the hydrolysis of the alkoxy groups in TMOS. The carbonyl stretching bands in PSI-SiO_2 hybrids (1776 and 1717 cm^{-1}) are shifted to a lower wave number as observed from a comparison with the 6B hybrid (1782 and 1724 cm^{-1}). This result indicates that a hydrogen bond is formed between the silanol groups and the carbonyl groups of polyimide in PSI-SiO_2 hybrids.[27]

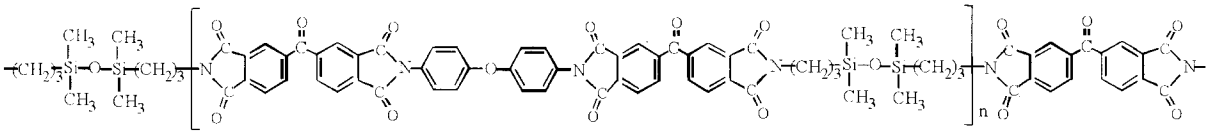

6B

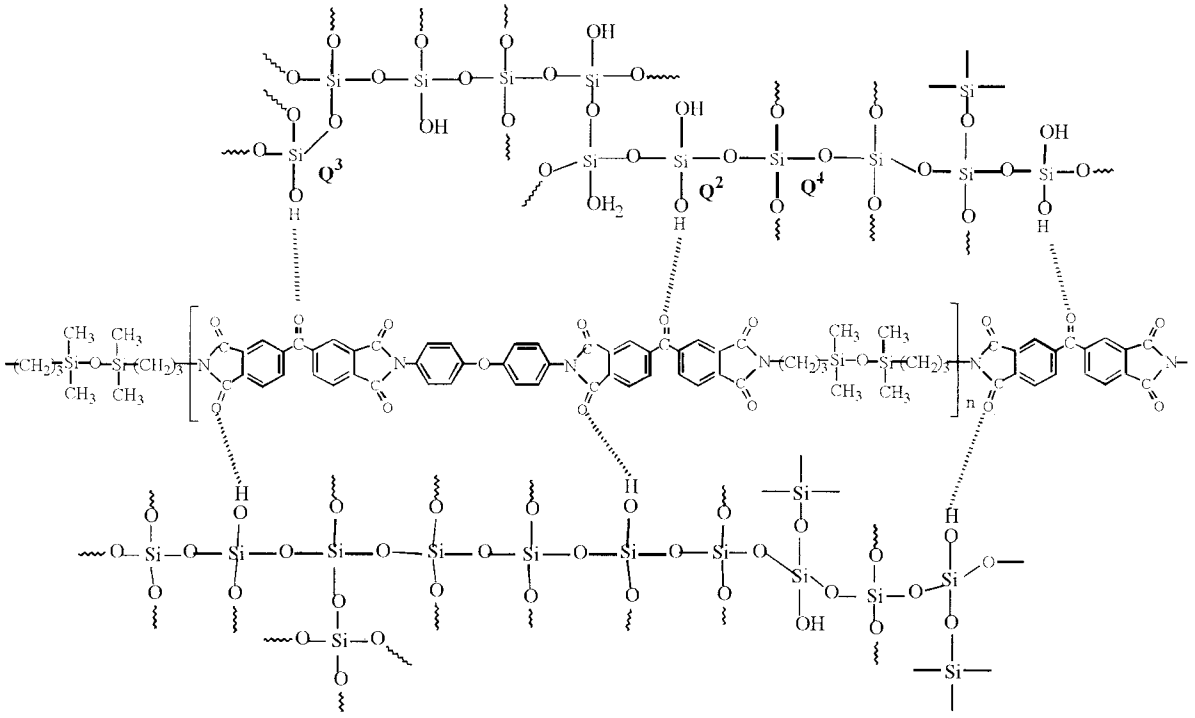

Figure 1 The theoretical structure of hybrid materials.

The ^{29}Si-NMR spectrum of the 6B hybrid has only one peak at 7.7 ppm [Fig. 3(A)] that is attributed to the silicon in the siloxane sequence. However, this band is shifted to ~ 14.5 ppm in PSI-SiO_2 hybrids [Fig. 3(B–F)], indicating that the silicon environments of silicon have changed. This may be due to the hydrogen bond that takes place between the PSI and the 3-D silica networks. Moreover, the other three peaks at about −90.6, −99.3, and −107.1 ppm are observed in PSI-SiO_2 hybrids that respectively corresponded to Q^2, Q^3, and Q^4 structures as shown in Figure 1. The parent silica has three peaks from Q^2, Q^3, and Q^4 silicon atoms at −90, −100, and −110 ppm, respectively, in the ^{29}Si-NMR spectrum.[28] The Q^4 resonance of hybrids deviates from the parent silica, indicating that interaction is created between the PSI and the silica.[29] This is further evidence of the existence of hydrogen bonds in PSI-SiO_2 hybrids. The relative proportions of the three kinds of silicon atoms are listed in Table II, which were determined by a quantitative analysis of the resonance signals. Interestingly, the degree of condensation decreases with increasing silica content. Moreover, the relative proportion of Q^3 increases with increasing silica content whereas that of Q^4 decreases. The results may be due to the fact that the coefficient of thermal expansion of the polyimide (~ 30 ppm/K) is larger than that of the silica (0.5 ppm/K).[21] However, the ^{29}Si-NMR spectra of hybrids 8B-50 and 10B-50 [Fig. 3(E, F)] are similar to that of 6B-50, and their degree of condensation is independent of the hydrolysis ratio (Table II). Consequently, the condensation reaction of the silanol groups in the PSI-rich hybrid 6B-30 is more completed than that in the silica-rich hybrid 6B-70. On the other hand, the peak width of siloxane

segments at half-height ($\nu_{1/2}$) in PSI-SiO_2 hybrids ($\sim$ 400 Hz, Table II) is broader than that in the 6B hybrid (295 Hz). This indicates that the silicon environment in the 6B hybrid is more homogeneous than in the PSI-SiO_2 hybrids.

Relaxation Properties

The ^{13}C-CP/MAS NMR spectrum of the 6B hybrid is shown in Figure 4. A set of peaks for polyimide are observed at around 193, 167, 154, and 140–118 ppm that arise from the benzophenone carbonyl, imide carbonyl, aryl carbons with oxygen substituents, and various aromatic carbons, respectively. Moreover, the other set of peaks are observed at around 41, 22, 15, and 0.93 ppm that correspond to —NCH_2—, —CH_2—, —CH_2Si—, and —$SiCH_3$, respectively. On the other hand, the $\nu_{1/2}$ of the hybrids ($\sim$ 350 Hz) in the ^{13}C-NMR spectra is broader than that of polyimide–siloxane block copolymers (66–200 Hz).[29] Therefore, the segments of imide and siloxane in the hybrid materials exhibit the fast Gaussian spin–spin relaxation that may be expressed by[23]

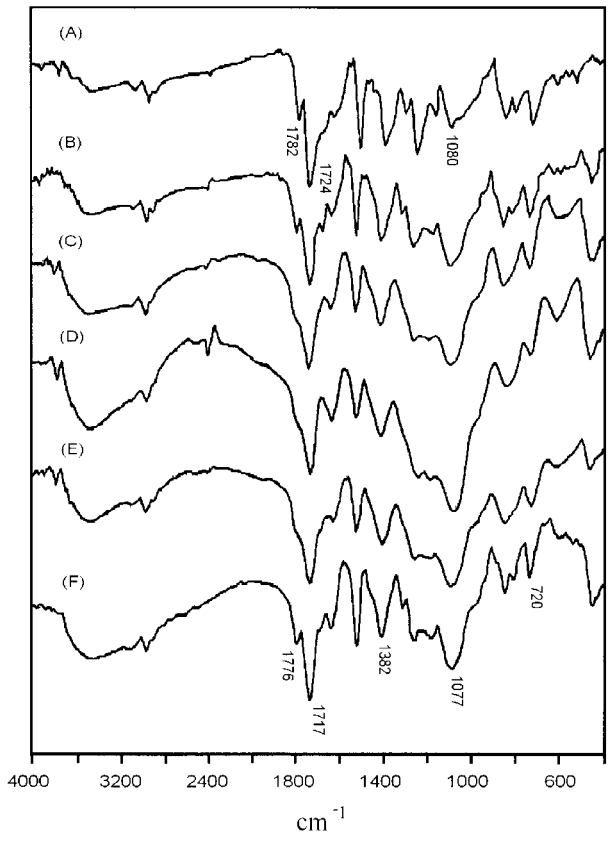

Figure 2 IR spectra of various hybrid materials: 6B (spectrum A), 6B-30 (spectrum B), 6B-50 (spectrum C), 6B-70 (spectrum D), 8B-50 (spectrum E), and 10B-50 (spectrum F).

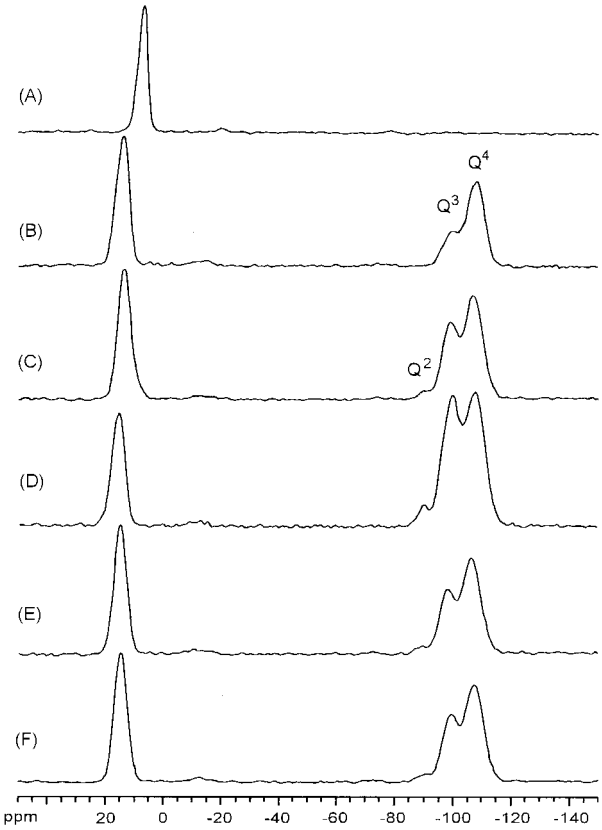

Figure 3 CP/MAS ^{29}Si-NMR spectra for 6B (spectrum A), 6B-30 (spectrum B), 6B-50 (spectrum C), 6B-70 (spectrum D), 8B-50 (spectrum E), and 10B-50 (spectrum F) hybrid materials.

$$I = \exp[-(\tau/T_2)^2/2] \quad (1)$$

where I, τ, and T_2 are the peak intensity, proton relaxation period, and spin–spin relaxation time, respectively.

Figure 5 shows the correlation between the ln I of the —$OSiCH_3$ peak in the ^{13}C-NMR spectra of the hybrids and the squared transverse (τ^2). The slopes of the straight lines yield the parameters T_2. This shows that the carbons of the siloxane segments exhibit two quasi-Gaussian fast decays. The T_2 values are at about 16 ($0 \leqq \tau^2 \leqq 600$) and 30 μs ($600 \leqq \tau^2 \leqq 1600$), respectively. This reveals that the mobility of the free siloxane chains is strongly restricted by the imide segments. On the other hand, the slopes of the straight lines in Figure 6 yield the fast T_2 ($0 \leqq \tau^2 \leqq 600$) and slow T_2 ($600 \leqq \tau^2 \leqq 1600$) parameters, respectively, corresponding to imide units in the sequence and interface. Therefore, the spin–spin relaxation of the rigid imide chain is affected by the flexible siloxane segments. However, the T_2 is indepen-

Table II Chemical Shift and Relative Proportions of Siloxane Units and Q^i in Hybrid Materials from ^{29}Si-NMR CP/MAS Spectra

Hybrids	Chemical Shifts (ppm)				Relative Proportions (%)			Degree of Condensation[a]
	Siloxane	Q^2	Q^3	Q^4	Q^2	Q^3	Q^4	
A: 6B	7.7 (295)[b]	—	—	—	—	—	—	—
B: 6B-30	14.2 (395)	—	−99.3	−107.7	—	28.8	71.2	92.8 (3.72)[c]
C: 6B-50	14.3 (403)	−90.6	−99.0	−106.8	4.2	40.9	54.9	87.7 (3.51)
D: 6B-70	14.6 (390)	−90.0	−99.5	−107.0	6.7	46.2	47.1	85.1 (3.40)
E: 8B-50	14.5 (398)	−90.6	−99.1	−107.1	4.7	38.5	56.8	88.0 (3.52)
F: 10B-50	14.5 (405)	−90.9	−99.4	−107.1	4.3	39.4	56.3	88.0 (3.52)

[a] Degree of condensation (%) = actual functionality × 100/potential functionality.
[b] The numbers in parentheses indicate the peak width at half-height (Hz).
[c] The numbers in parentheses indicate the actual functionality.

dent of the silica contents and hydrolysis ratio (Table III). This indicates that the chain mobility of the PSI segments is minimally affected by hydrogen bonding in the hybrids.

Thermal Analysis

The TGA curves of hybrid materials in air are shown in Figure 7, which are reflected in two main peaks in differential TG (DTG) weight loss curves. The weight losses below 350°C, corresponding to the release of methanol and water during heating,[30] increased as the TMOS content increases. This indicates that the sol–gel process is incomplete.[30] The degradation in the first (400–550°C) and second stage (550–700°C) of the DTG curves correspond to the decomposition of organic siloxane and the imide, respectively.[26] The final weight residue (Y_c) at 800°C is constituted of silica, and that is proportional to the TMOS content. The T_{1m} and T_{2m} represent the maximum rate temperature of weight loss at the first and second stage, respectively. The degradation parameters of hybrids at a heating rate of 10°C/min are listed in Table IV. The data show that the T_{1m} and T_{2m} of PSI-SiO_2 hybrids in thermooxidative degradation are smaller than that of the 6B hybrid. Moreover, the T_{1m} and Y_c of PSI-SiO_2 hybrids increase with increasing silica content, but the T_{2m} is less dependent on the silica content and its value is around 630°C. In addition, the thermooxidative degradation parameters of 8B-50 and 10B-50 (Table IV) are not

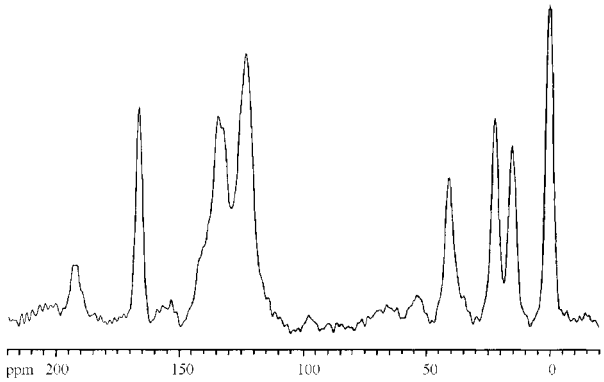

Figure 4 The ^{13}C-NMR CP/MAS spectrum of the 6B hybrid.

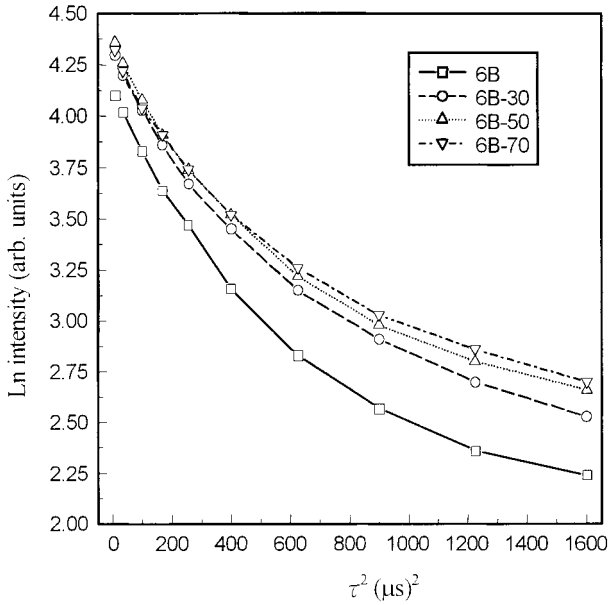

Figure 5 The logarithmic intensity (arb. units) of the CP/MAS ^{13}C-NMR spectra of siloxane segments in various silica proportions in the hybrid materials versus the square of the proton relaxation period (τ^2).

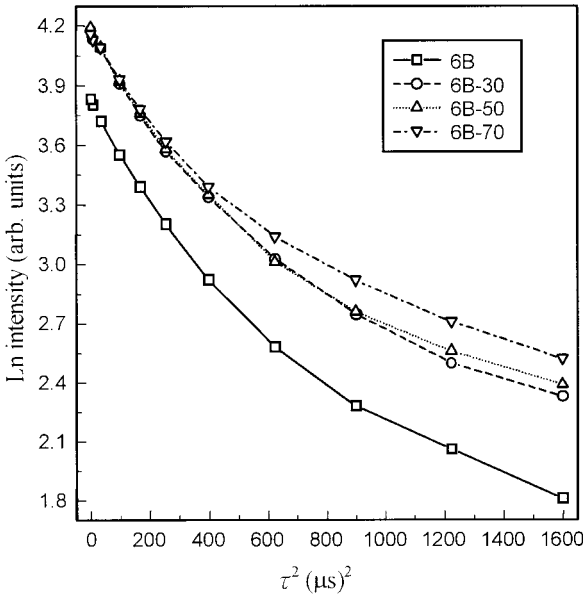

Figure 6 The logarithmic intensity (arb. units) of the CP/MAS ^{13}C-NMR spectra of polyimide segments in various water proportions in the hybrid materials versus the square of the proton relaxation period (τ^2).

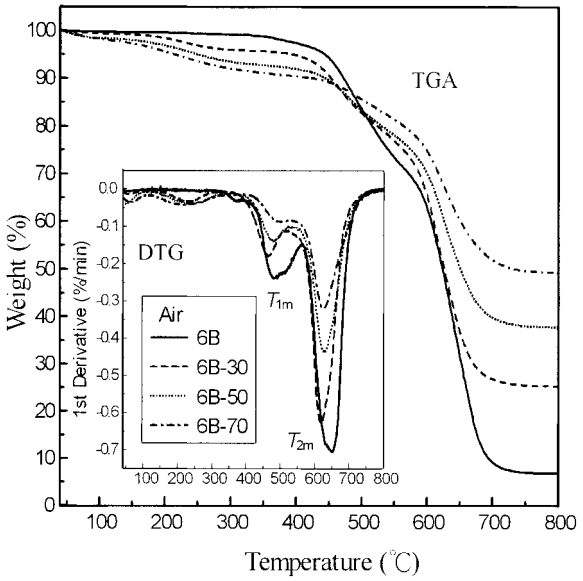

Figure 7 The TGA and DTG thermograms of hybrid materials in air at a heating rate of 10°C/min.

markedly different from 6B-50. The results indicate that the silica has some influence on the thermooxidative stability of the hybrids.

The TGA curves of the hybrids under nitrogen are shown in Figure 8, which reflects more than three peaks in the DTG weight loss curves. A standard line shape analysis above 400°C with multiple Gaussian fitting functions reveals that the DTG curve of the hybrids can be fitted by three degraded steps.[31] The peak temperatures of each stage of degradation in the 6B hybrid are about 510 (T_{1m}), 650 (T_{2m}), and 750°C (T_{3m}), which are attributed to scissions of aliphatic *n*-propyl segments, siloxane-connected imide, and more stable imide segments, respectively. However, the relative proportion of the third degradation stage to the second stage decreases with increasing silica content (Fig. 8). Note that the Y_c values in the thermal degradation are comparable to that in thermooxidative degradation, indicating that the PSI segments in PSI-SiO_2 hybrids are in nearly complete decomposition. These results reveal that silica increases the degradation of the imide segments.

Kinetic Analysis

The reaction order (n) for thermooxidative degradation of hybrids in this work was determined by the Kissinger equation.[32]

$$n = 1.26\sqrt{S} \tag{2}$$

Here S is the shape index of the DTG analysis. The shape index is defined as the absolute value

Table III Chemical Shifts (δ), Peak Width at Half-Height ($\nu_{1/2}$), and Spin–Spin Relaxation Time (T_2) Values of Different Segmented Hybrid Materials under ^{13}C-NMR Analysis

	Siloxane Phase				Imide Phase			
Hybrids	δ (ppm)	$\nu_{1/2}$ (Hz)	T_2 (μs)		δ (ppm)	$\nu_{1/2}$ (Hz)	T_2 (μs)	
A: 6B	0.72	348	15.5	28.9	166.6	314	15.7	25.5
B: 6B-30	0.18	352	16.4	29.4	166.7	357	16.4	26.5
C: 6B-50	−0.26	353	16.6	29.9	166.7	343	16.2	27.9
D: 6B-70	−0.41	333	17.2	30.4	167.0	362	17.0	28.6
E: 8B-50	−0.40	353	16.3	29.1	166.9	356	16.8	26.4
F: 10B-50	−0.12	356	16.5	28.9	166.8	368	16.6	25.6

Table IV Characteristic Parameter of Degradation (10°C/min) for Hybrid Materials

	Air			N_2			Siloxane Phase		Imide Phase	
Hybrids	T_{1m}	T_{2m}	Y_c	T_{1m}	T_{2m}	Y_c	n	E_a	n	E_a
A: 6B	500	650	7	510	650	10	1.25	94	1.20	162
B: 6B-30	465	620	26	500	644	27	1.21	76	1.29	159
C: 6B-50	480	629	38	500	651	37	1.23	58	1.26	137
D: 6B-70	500	630	50	509	661	51	1.28	45	1.28	124
E: 8B-50	488	632	36	523	665	40	1.28	58	1.34	139
F: 10B-50	484	632	36	530	670	46	1.23	60	1.30	140

T_{1m} and T_{2m}, the maximum rate temperature (°C) of weight loss at the first and second stage; Y_c, char yield (wt %) at 800°C; n, decomposition order; E_a, apparent activation energy (kJ/mol) in air.

of the ratio of the slopes of tangents to the curve at the inflection points. The n values in thermooxidative degradation for the hybrids are listed in Table IV. The degree of conversion (α) is defined as the ratio of the actual weight loss to the total weight loss. For $n \neq 1$, the integrated form of the rate of degradation $g(\alpha)$ is given by eq. (3).

$$g(\alpha) = [1 - (1 - \alpha)^{1-n}]/(1 - n) \quad (3)$$

The method of calculation of the apparent activation energy (E_a) for the hybrids' degradation was proposed by van Krevelen.[22] This method for solving the integral of eq. (3) can be derived as follows:

$$\ln g(\alpha) = \ln[A(0.368/T_m)^x/q(\chi + 1)] + (\chi + 1)\ln T \quad (4)$$

Here A, T, q, and χ represent the preexponential factor, temperature, heating rate, and $\chi = E_a/RT_m$. A plot of the $\ln g(\alpha)$ versus $\ln T$ gives a straight line (Fig. 9). It is possible to calculate the activation energies of thermooxidative degradation for siloxane and imide segments from the slopes of the straight line. Table IV summarizes the activation energies of thermooxidative degradation for hybrids. We found that the E_a values for siloxane and polyimide segments decrease with increasing silica content, but the E_a is less dependent on the hydrolysis ratio. The results reveal that silica may favor the aliphatic n-propyl segments[33] and the imide segment's degradation.

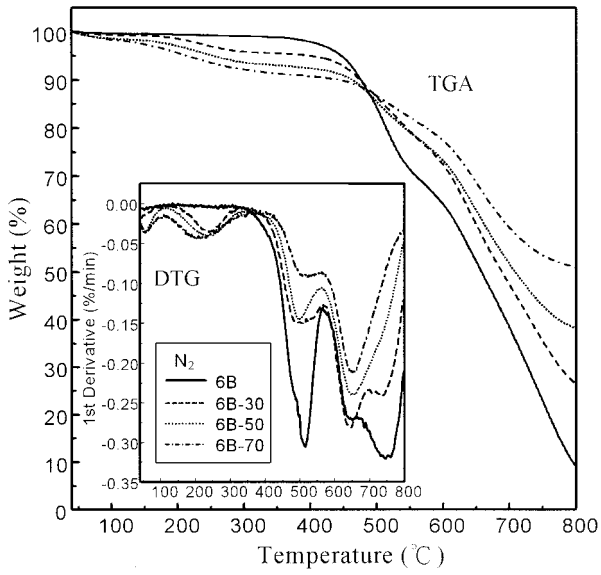

Figure 8 The TGA and DTG thermograms of hybrid materials in N_2 at a heating rate of 10°C/min.

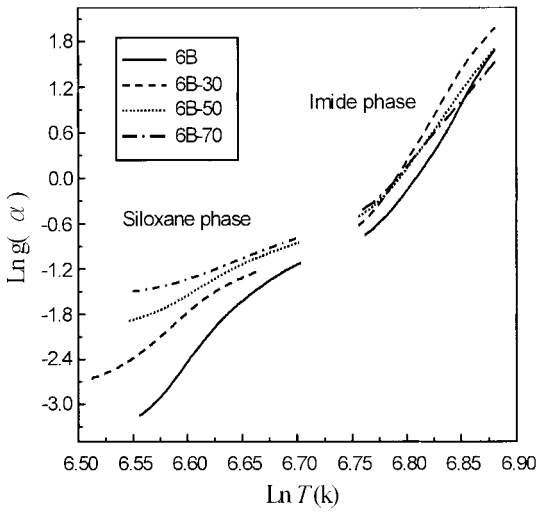

Figure 9 A plot of $\ln g(\alpha)$ versus $\ln T$ for thermooxidative degradation of siloxane and imide segments in the hybrids in air at 10°C/min.

This may be associated with the higher thermal conductivity of the silica (5 mcal/cm s °C) than that of polyimide (0.4 mcal/cm s °C).[34]

CONCLUSIONS

The PSI-SiO_2 hybrid materials were prepared via polycondensation, polyimidization, and sol–gel techniques by mixing TMOS with a BTDA-ODA-DAPrTMDS PSI precursor. Various proportions of TMOS and various hydrolysis ratios were used. The interaction between silica and PSI was confirmed through IR and ^{29}Si-NMR. Four components with different molecular mobilities in the hybrids were observed by spin–spin relaxation measurements. The E_a values of thermooxdative degradation in the hybrids were evaluated by the van Krevelen method. The molecular mobility of the siloxane and imide segments was independent of the silica content and hydrolysis ratio. However, the E_a of the siloxane and imide segments decreased with increasing silica content. The results suggested that the higher thermal conductivity of silica may favor the degradation of the siloxane and imide segments.

We thank Miss S. Y. Fang (Tsing Hua University) for help in the NMR measurements and Mr. Y. C. Lin (Chung Shan Institute of Science and Technology) for help in the TGA measurements.

REFERENCES

1. Mark, J. E.; Lee, C. Y. C.; Bianconic, P. A., Eds. Hybrid Organic–Inorganic Composites; ACS Symposium Series 585; American Chemical Society: Washington DC, 1995.
2. Morikawa, A.; Iyoku, Y.; Kakimoto, M.; Imai, Y. J Mater Chem 1992, 2, 679.
3. Mark, J. E.; Jiang, C. J.; Tang, M. Y. Macromolecules 1984, 17, 2613.
4. Glaser, R. H.; Wilkes, G. L. Polym Bull 1988, 19, 51.
5. Fujita, M.; Honda, K. Polym Commun 1989, 30, 200.
6. Wang, B.; Wilkes, G. L.; Hedrick, J. C.; Liptak, S. C.; McGrath, J. E. Macromolecules 1991, 24, 3449.
7. Philipp, G.; Schmidt, H. J Non-Cryst Solids 1984, 63, 283.
8. Theberge, E. Polym Plast Technol Eng 1981, 16, 41.
9. Nandi, M.; Conklin, J. A.; Salviati, J. L.; Sen, A. Chem Mater 1990, 2, 772.
10. Breval, E.; Mulvihill, M. L.; Dougherty, J. P.; Newnham, R. E. J Mater Sci 1992, 27, 3297.
11. Morikawa, A.; Iyoku, Y.; Kakimoto, M.; Imai, Y. Polym J 1992, 24, 107.
12. Morikawa, A.; Yamaguchi, H.; Kakimoto, M.; Imai, Y. Chem Mater 1994, 6, 913.
13. Gaw, K.; Suzuki, H.; Kakimoto, M.; Imai, Y. Mater Res Soc Symp Proc 1996, 6, 435.
14. Goizet, S.; Schrotter, J. C.; Smaihi, M.; Deratani, A. New J Chem 1997, 21, 461.
15. Mascia, L.; Kioul, A. J Mater Sci Lett 1994, 13, 641.
16. Wang, S.; Ahmad, Z.; Mark, J. E. Macromol Rep 1994, A31, 411.
17. Mascia, L.; Kioul, A. Polymer 1995, 36, 3649.
18. Beecroft, L. L.; Johnen, N. A.; Ober, C. K. Polym Adv Technol 1997, 8, 289.
19. Sysel, P.; Pulec, R.; Maryska, M. Polym J 1997, 29, 607.
20. Sroog, C. A. Progr Polym Sci 1991, 16, 561.
21. Numata, S.; Kinjo, N. Polym Eng Sci 1988, 28, 906.
22. Van Krevelen, D. W.; Van Herden, C.; Huntjens, F. J. Fuel 1951, 30, 253.
23. Tékély, P.; Canet, D.; Delpuech, J. J. Mol Phys 1989, 67, 81.
24. Feng, H.; Shi, L.; Feng, Z.; Shen, L. Makromol Chem 1993, 194, 2257.
25. Avadhani, C. V.; Chujo, Y.; Kuraoka, K.; Yazawa, T. Polym Bull 1997, 38, 501.
26. Wu, K. H.; Chang, T. C.; Wang, Y. T.; Chiu, Y. S. J Polym Sci Polym Chem 1999, 37, 2275.
27. Ahn, T.; Kim, M.; Choe, S. Macromolecules 1997, 30, 3369.
28. Joseph, R.; Zhang, S.; Ford, W. T. Macromolecules 1996, 29, 1305.
29. Chang, T. C.; Wu, K. H. Polym Degrad Stabil 1998, 60, 161.
30. Kioul, A.; Mascia, L. J Non-Cryst Solids 1994, 175, 169.
31. Chang, T. C.; Liao, C. L.; Wu, K. H.; Chiu, Y. S. Polym Degrad Stabil 1999, 64, 227.
32. Kissinger, H. H. E. Anal Chem 1957, 29, 1702.
33. Yilgor, I.; McGrath, J. E. Adv Polym Sci 1988, 86, 1.
34. Soane, D. S.; Martynenko, Z. Polymers in Microelectronics, Fundamentals and Applications; Elsevier: Amsterdam, 1989; p. 159.